Journal of Petroleum Science and Engineering 166 (2018) 242–248

Contents lists available at ScienceDirect

Journal of Petroleum Science and Engineering

journal homepage: www.elsevier.com/locate/petrol

Fast and accurate simulation of electromagnetic telemetry in deviated and horizontal drilling

Shubin Zeng, Dawei Li, Donald R. Wilton, Jiefu Chen *

University of Houston, Houston, TX, USA

ARTICLE INFO

Keywords:
Deviated and horizontal drilling
Electromagnetic telemetry
Integral equations
Layered medium Green's function
Thin wire kernel

ABSTRACT

Electromagnetic (EM) telemetry systems are widely used for measurement-while-drilling (MWD), especially in unconventional drilling. In this paper, a numerical method for the simulation of EM telemetry systems in deviated and horizontal drilling is introduced. The underground formation is assumed to be horizontally layered media, and the long, metal drill string acts as an antenna that may be treated as a thin wire excited by a gap voltage source located near the drill bit. The numerical model employs the electric field integral equation (EFIE) and the method of moments (MoM) to obtain a linear system for the axial current distribution on the drill string, which is subdivided into several one-dimensional segments. By using the thin wire kernel, near-field interactions can be evaluated accurately and efficiently, while also reducing problem dimensionality and singularity order of the homogeneous medium contribution to the layered medium Green's function (LMGF). The latter typically takes the form of a dyadic spectral domain integral, the asymptotics of whose integrands may be estimated and combined with Kummer's method to accelerate its evaluation, with the asymptotic correction terms evaluated in closed or easily evaluated forms. Numerical results are presented to verify the fast and accurate performance of the proposed approach. Results for signal voltage receivability by a surface antenna are also presented and discussed.

1. Introduction

Measurement-while-drilling (MWD) telemetry is a technology that can transmit data from downhole sensors to surface while an oil well is being drilled. Electromagnetic (EM) telemetry systems use electromagnetic means to transmit data from downhole to the surface in real time, with a surface antenna to detect the voltage signal and equipment to decode the data. EM telemetry helps operators optimize the drilling path to improve production.

Different methods (Hill and Wait, 1978; Bhagwan and Trofimenkoff, 1982; DeGauque et al., 1987) have been proposed to model EM telemetry systems in the literature. Early modeling was limited to vertical wells in homogeneous earth formations. In 1993, Xia and Chen (Xia and Chen, 1993) applied the electric field integral equation (EFIE) to both vertical and deviated wells, however, the earth model is always assumed to be two half spaces. In 2009, Yang (Yang et al., 2009) employed the EFIE approach and method of moments (MoM) (Harrington and Harrington, 1996) to discretize the thin casing in horizontally layered media into one-dimensional (1D) segments solved for the electric current distribution along the steel-cased well. This method removed the restriction of homogeneous media by calculating unknown coefficients determined by enforcing the continuity of tangential EM fields at layer interfaces. However, this approach was confined to vertical wells in layered media. More recently, Wei (Wei et al., 2010) developed a numerical method to obtain the current distribution along an arbitrarily oriented drill string in layered media, but a constant angle of deviation from the vertical direction was assumed. Other numerical methods, such as the semi-analytical finite element method (FEM) (Chen et al., 2017) and numerical matching method (NMM) (Li et al., 2014), have also been reported for modeling EM telemetry systems of vertical wells in layered formations, with limited applications. To the best of our knowledge, an efficient simulation algorithm of EM telemetry in horizontal and deviated drilling in layered media has not been published.

In practice, the operation of drilling the well will induce some noise for EM telemetry. To enhance the ratio of signal to noise, several methods (Li et al., 2016; Zeng et al., 2017; Jannin et al., 2017) have been proposed and show better performance over conventional EM telemetry.

In this paper, our objective is to develop a fast and accurate numerical method for the simulation of EM telemetry systems for drill strings of arbitrary 3D trajectories in horizontally layered media. The drill string is modeled as a thin wire antenna discretized into 1D segments. Then a mixed-potential integral equation (MPIE) form of the EFIE and MoM are

* Corresponding author.
E-mail address: jchen84@uh.edu (J. Chen).

https://doi.org/10.1016/j.petrol.2018.03.025
Received 15 February 2017; Received in revised form 30 January 2018; Accepted 5 March 2018
Available online 8 March 2018

employed to obtain a linear system for the axial current distribution on the drill string. To obtain the electric field induced by the drill string current, the layered media Green's function (LMGF) (Michalski and Zheng, 1990) is used to calculate the magnetic vector and electric scalar potentials appearing in the MPIE. The proposed numerical method can quickly and accurately evaluate the potentials induced by arbitrarily oriented electric currents, thus providing a way to simulate the current distribution on drill strings for both deviated and horizontal drilling. After introducing the numerical simulation method, we benchmark the numerical results with COMSOL and consider some examples for the receivability of voltage signals in an EM telemetry system for directional drilling.

2. Methodology

Fig. 1 shows a schematic of an electromagnetic telemetry system for directional drilling. A transmitter near the drill bit is implemented as a voltage source. The surrounding formation is horizontally layered and resistive. When EM field propagates from the source to the surface through the formation and the steel pipe, the strength of EM field will be attenuated. To obtain the accurate voltage signal received by the surface antenna, we formulate the problem in the frequency domain as an EFIE:

$$[\mathbf{E}^i(\mathbf{r}) + \mathbf{E}^s(\mathbf{r})]_{tan} = Z_s \mathbf{J}_s, \quad \mathbf{r} \in S, \tag{1}$$

where S denotes the surface of the drill string, Z_s denotes the surface impedance of the drill string, and $\mathbf{J}_s$ denotes the axial surface current on drill string. If we assume the drill string is a perfect conduction, then Z_s vanishes. If the conductivity of drill string is finite, we can assign a specific value to Z_s (DeGauque et al., 1987). The excitation $\mathbf{E}^i(\mathbf{r})$ is a voltage gap source near the drill bit, as shown in Fig. 1. The secondary or scattering electric field $\mathbf{E}^s(\mathbf{r})$ can be expressed in terms of magnetic vector and electric scalar potentials at point $\mathbf{r}$ on the surface of the drill string using the mixed-potential formula

$$\mathbf{E}^s(\mathbf{r}) = -j\omega\mathbf{A}(\mathbf{r}) - \nabla\Phi(\mathbf{r}), \tag{2}$$

where ω is the angular frequency.

Since low frequencies are required for telemetry, the drill string has an electrically small radius that may be treated by thin-wire theory.

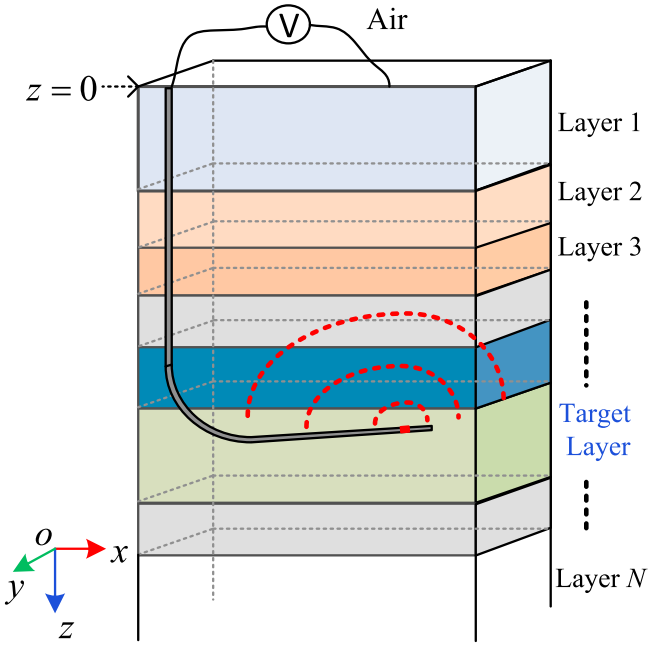

Fig. 1. Schematic of EM telemetry system in layered media.

Accordingly, the drill string surface current is assumed to be axially-directed and azimuthally invariant. Furthermore, $\mathbf{r}$ in (2) and the following can be placed on the wire axis and a radial vector of length equal to the drill string radius added to reach a single point on the drill string surface S; the latter, small vector may be safely ignored for points more than a few pipe radii away from source points $\mathbf{r}'$. The drill string potentials in layered media for electric current sources can be expressed in terms of a mixed-potential form of LMGF (MPGF):

$$\mathbf{A}(\mathbf{r}) = \mu_0 \int_S \mathcal{G}^A(\mathbf{r},\mathbf{r}') \cdot \frac{\mathbf{I}(\mathbf{r}')}{2\pi a(\mathbf{r}')} dS', \tag{3}$$

$$\Phi(\mathbf{r}) = -\frac{1}{j\omega\varepsilon_0}\left[\int_S K^\Phi(\mathbf{r},\mathbf{r}')\nabla' \cdot \frac{\mathbf{I}(\mathbf{r}')}{2\pi a(\mathbf{r}')} dS' + \int_S P_z(\mathbf{r},\mathbf{r}')\hat{\mathbf{z}} \cdot \frac{\mathbf{I}(\mathbf{r}')}{2\pi a(\mathbf{r}')} dS'\right], \tag{4}$$

where ε_0 and μ_0 denote the permittivity and permeability in free space, respectively. $a(\mathbf{r}')$ is the radius of the drill string at source point $\mathbf{r}'$ on S, and $\mathbf{I}(\mathbf{r}')$ denotes the total axial current. Since these latter quantities are assumed to be constant in a thin wire cross section, $\mathbf{r}'$ may also be taken as a point along the drill string axis in these terms; in the kernel quantities, $\mathbf{r}'$ generally is the axis point plus a small radial vector of radius $a(\mathbf{r}')$ to S. Components of the dyadic Green's function (DGF) $\mathcal{G}^A$ physically represent the components of the magnetic vector potential at $\mathbf{r}$ for the variously-oriented unit-strength electric current dipoles at $\mathbf{r}'$. K^Φ is the corresponding scalar potential kernel, and P_z is the vertical current scalar potential correction factor for layered media (Michalski and Zheng, 1990).

In homogeneous media with wavenumber k, the LMGF will be simplified to terms with the well-known scalar Green's function,

$$G(\mathbf{r},\mathbf{r}') = \frac{e^{-jkR}}{4\pi R}, \tag{5}$$

where $R = |\mathbf{r} - \mathbf{r}'|$. Indeed, in homogeneous media $\mathcal{G}^A = \mathcal{I}\, G(\mathbf{r},\mathbf{r}')$ ($\mathcal{I}$ is the identity dyad), $K^\Phi = G(\mathbf{r},\mathbf{r}')$, and $P_z = 0$. In layered media, $G(\mathbf{r},\mathbf{r}')$ or its related derivatives and integrals, are asymptotic limits of the MPGFs near source regions. When these "direct" contributions are removed from the MPGFs, all other contributions are non-singular and arise from boundary reflections (in the source layer) or from cross-boundary transmissions (in source-free layers). These kernel asymptotic forms, including associated quasi-static images forms, may be used in conjunction with Kummer's method to simultaneously accelerate the spectral integrals and isolate their singularities outside the spectral integral when observation source points, $\mathbf{r}$ and $\mathbf{r}'$, respectively, are close or coincide. Furthermore, azimuthal integration on source points at a drill string cross section then simply replaces such terms with the so-called thin-wire kernel (Wilton and Champagne, 2006)

$$K(\mathbf{r},\mathbf{r}') = \frac{1}{2\pi}\int_{-\pi}^{\pi} G(\mathbf{r},\mathbf{r}')d\phi', \tag{6}$$

or its related derivatives or integrals. All remaining spectral difference potential kernels either vanish or are slowly varying about the drill string axis; for them, $\mathbf{r}'$ can be a point on the drill string axis in (3) and (4). Thus the circumferential integration and all effects of pipe radius are isolated to terms containing (6).

In layered media, we must evaluate three types of LMGFs (Michalski and Zheng, 1990), i.e., $\mathcal{G}^A$, K^Φ, and P_z. Most of the LMGF evaluation effort occurs in the spectral domain where we employ the Fourier transform pair

$$\tilde{\mathcal{F}}(\mathbf{k}_\rho) = \int_{-\infty}^{\infty}\int_{-\infty}^{\infty} \mathcal{F}(\mathbf{k}_\rho) e^{j\mathbf{k}_\rho \cdot \boldsymbol{\rho}} dxdy, \tag{7}$$

$$\mathscr{F}(\boldsymbol{\rho}) = \frac{1}{(2\pi)^2}\int_{-\infty}^{\infty}\int_{-\infty}^{\infty}\tilde{\mathscr{F}}(\mathbf{k}_\rho)e^{-j\mathbf{k}_\rho\cdot\boldsymbol{\rho}}dk_x dk_y, \tag{8}$$

where $\mathscr{F}$ may be a scalar, vector, or dyadic quantity and $\boldsymbol{\rho} = x\hat{\mathbf{x}} + y\hat{\mathbf{y}}$ is the transverse component of the position vector $\mathbf{r}$. By decomposing the transformed fields and potentials into transverse and longitudinal components in the spectral domain, we obtain transmission line analogs of Maxwell's equations in layered media. The overall approach, known as the spectral domain immittance (SDI) method (Itoh, 1980), splits the electromagnetic fields into transverse magnetic (TM) transverse electric (TE) fields, each with its spectral transverse equivalent network (TEN) representation (Felsen and Marcuvitz, 1994). The MPGFs in the spectral domain are obtained as (Michalski and Mosig, 1997)

$$\tilde{\mathscr{G}}^A(\mathbf{k}_\rho, z, z') = \begin{bmatrix} \frac{1}{j\omega\mu_0}V_i^h & 0 & 0 \\ 0 & \frac{1}{j\omega\mu_0}V_i^h & 0 \\ \frac{\mu_r k_x}{jk_\rho^2}\left(I_i^h - I_i^e\right) & \frac{\mu_r k_y}{jk_\rho^2}\left(I_i^h - I_i^e\right) & \frac{\mu_r}{j\omega\varepsilon_0\varepsilon'_{rc}}I_v^e \end{bmatrix} \tag{9}$$

$$\tilde{K}^\Phi(\mathbf{k}_\rho, z, z') = -j\omega\varepsilon_0\frac{V_i^h - V_i^e}{k_\rho^2}, \tag{10}$$

$$\tilde{P}_z(\mathbf{k}_\rho, z, z') = \frac{k_0^2\mu_r'}{k_\rho^2}\left(V_v^h - V_v^e\right), \tag{11}$$

where $\mathbf{k}_\rho = k_x\hat{\mathbf{x}} + k_y\hat{\mathbf{y}}$, with z and z' denoting the longitudinal components of $\mathbf{r}$ and $\mathbf{r}'$, respectively. Material parameter μ_r is the relative magnetic permeability and $\varepsilon_{rc} = \varepsilon_r - j\sigma/\omega\varepsilon_0$ is the relative complex or effective permittivity; ε_r is the relative dielectric permittivity and σ is the formation conductivity. Note that unprimed relative material parameters in (9)–(11) are evaluated at observation points z, while corresponding primed quantities are evaluated at source points z'.

Quantities V_β^α and I_β^α, $\alpha = e, h$ and $\beta = v, i$, are transmission line voltages and currents, respectively, evaluated at observation points z and are due to unit-strength voltage or current sources located at points z'. Superscripts e and h denote TM and TE wave polarizations, respectively, while subscripts v and i denote the unit-strength source types, voltage or current, respectively. These voltages and currents are merely (scalar) transmission line Green's functions (TLGF) that can be determined by the method of (Michalski and Mosig, 1997). Since the angular variation of the MPGFs are relatively simple, the doubly-infinite inverse Fourier transform (IFT) integrals of (9)–(11) may be more efficiently evaluated as Hankel transforms,

$$S_n\left\{\tilde{\mathscr{F}}(\mathbf{k}_\rho)\right\} = \frac{1}{2\pi}\int_0^\infty \tilde{\mathscr{F}}(\mathbf{k}_\rho)J_n\left(k_\rho|\boldsymbol{\rho} - \boldsymbol{\rho}'|\right)k_\rho\, dk_\rho, \tag{12}$$

where J_n is the Bessel function of the first kind, order n, and $\boldsymbol{\rho}$ and $\boldsymbol{\rho}'$ denote the transverse components of $\mathbf{r}$ and $\mathbf{r}'$, respectively. This reduces the IFT to a single semi-infinite integral, and (12) is known as a Sommerfeld-type integral (Sommerfeld, 1949). The spatial domain form of the MPGF can finally be expressed as

$$\mathscr{G}^A(\boldsymbol{\rho} - \boldsymbol{\rho}', z, z') = \begin{bmatrix} \frac{1}{j\omega\mu_0}S_0\left\{V_i^h\right\} & 0 & 0 \\ 0 & \frac{1}{j\omega\mu_0}S_0\left\{V_i^h\right\} & 0 \\ -\mu_r\cos\gamma S_1\left\{\frac{I_i^h - I_i^e}{k_\rho}\right\} & -\mu_r\sin\gamma S_1\left\{\frac{I_i^h - I_i^e}{k_\rho}\right\} & \frac{\mu_r}{j\omega\varepsilon_0\varepsilon_{rc}}S_0\left\{I_v^e\right\} \end{bmatrix} \tag{13}$$

$$K^\Phi(\boldsymbol{\rho} - \boldsymbol{\rho}', z, z') = -j\omega\varepsilon_0 S_0\left\{\frac{V_i^h - V_i^e}{k_\rho^2}\right\}, \tag{14}$$

$$P_z(\boldsymbol{\rho} - \boldsymbol{\rho}', z, z') = k_0^2\,\mu'_r S_0\left\{\frac{V_v^h - V_v^e}{k_\rho^2}\right\}, \tag{15}$$

where

$$\gamma = \tan^{-1}\left(\frac{y - y'}{x - x'}\right). \tag{16}$$

For reasonably thick layers and z and z' not in the same or adjacent layers, the Hankel transform integrals converge exponentially, but when they are in the same or adjacent layers, evaluation of each spatial component of the MPGF may be accelerated by subtracting the appropriate spectral asymptotic form and adding back its Hankel transform evaluation as a closed or easily evaluated form (Champagne, 1996). The resulting difference integrands in (12) thus take the form

$$\Delta F(\boldsymbol{\rho} - \boldsymbol{\rho}', z, z') \equiv F(\boldsymbol{\rho} - \boldsymbol{\rho}', z, z') - F^\infty(\boldsymbol{\rho} - \boldsymbol{\rho}', z, z'), \tag{17}$$

where the last term in (17) is an appropriate asymptotic form of the spectral MPGF whose Hankel transform has a closed or easily-evaluated form.

The thin wire kernel (6) and related homogeneous media forms can be used to evaluate the asymptotic forms of $\mathscr{G}^A$, K^Φ, and P_z since they are all closed or easily evaluated forms related to (5) (Yla-Oijala and Taskinen, 2003). However, the Sommerfeld difference integrands on the left side of (17) must be numerically evaluated using an adaptive Romberg quadrature applied on each segment of a deformed path shown in Fig. 2 that skirts possible poles near the axis. The semi-infinite tail integrals of the path are evaluated using an extrapolation method such as the weighted average method (WAM) (Michalski, 1998).

The numerical solution of the electric current distribution on the drill string is solved by MoM. The drill string is discretized as $(N + 1)$ linear segments with N interior nodes only since current vanishes at the drill string endpoints. Then the unknown current $\mathbf{I}(\mathbf{r})$ is approximated as

$$\mathbf{I}(\mathbf{r}) = \sum_{n=1}^{N} I_n\boldsymbol{\Lambda}_n(\mathbf{r}), \quad \mathbf{r} \in S. \tag{18}$$

Since the drill string is thin, the linearly-interpolating vector basis functions $\boldsymbol{\Lambda}_n(\mathbf{r})$ have only an axially-directed component with I_n as the unknown current through the n-th node.

The EFIE is transformed into matrix form by inserting Eqs. (2)–(4), (13)-(15), and (18) into Eq. (1) and applying the Galerkin form of the MoM, yielding

$$([Z_{mn}] + [Z_s])[I_n] = \left[V_n^i\right], \tag{19}$$

where $[Z_{mn}]$ represents the mutual impedance between segments containing nodes m and n, respectively, $[Z_s]$ is a diagonal matrix

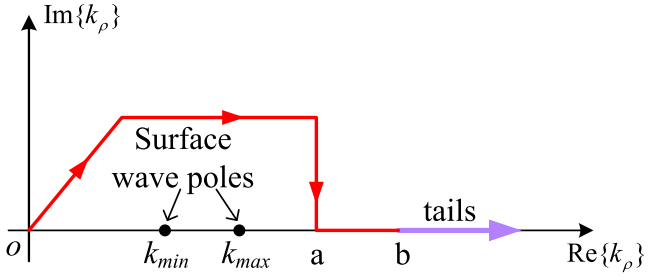

Fig. 2. Numerical integration path for Sommerfeld integrals in the complex k_ρ plane.

corresponding to the surface impedance of the drill string, and $[V_n^i]$ corresponds to the impressed voltage at the source gap. Upon solving the linear system (19) for the current distribution on the drill string, it is then straightforward to numerically integrate the electric field along the formation surface using (2) to obtain the voltage signal received at a surface antenna.

3. Numerical examples

In this section, several sample models are studied using the proposed numerical method. To verify the accuracy of the method, we first benchmark the programmed code against solutions obtained using COMSOL, whose solver uses FEM, for both a vertical and a horizontal well. The layered formation is below the $z = 0$ plane; the region above is air.

Fig. 3 shows a drill string inserted vertically into a five-layer formation. The relative dielectric permittivity and relative magnetic permeability in each layer are unity, while the resistivities of Layers 1–5 are 100 Ω· m, 20 Ω· m, 10 Ω· m, 5 Ω· m and 100 Ω· m, respectively. The total length of the drill string is 5000 ft. The thicknesses of Layers 1–4 are 500 ft, 1500 ft, 2500 ft and 1000 ft, respectively, while Layer 5 extends from $z = 5500$ ft to infinity. A 1-V voltage source is placed at $z = 4750$ ft and the operating frequency of the source is 5 Hz. The radius of the drill string is 5 in. As shown in Fig. 4, the computed electric current distribution along the drill string is in excellent agreement with the corresponding results obtained by COMSOL when the drill string is perfect electric conductor (PEC) or of finite conductivity ($\sigma = 10^5$ S/m). The finite conductivity of the drill string can have a substantial impact on both the magnitude and phase of the current distribution. Different resistivities in each layer can introduce different rates of decay for the current on the drill string. By comparing the current distributions of 500–2000 ft and 2000–4500 ft in Fig. 4, we can observe that smaller resistivity leads to larger rate of decay while larger resistivity leads to relatively smaller attenuation.

To validate our method for horizontal or deviated drilling, the simulation of a horizontal well with total 6000 m measured depth has been studied using both our method and COMSOL. The geometry of the horizontal well and surrounding formation are shown in Fig. 5. The formation has five layers with different resistivities and thicknesses as labelled in Fig. 5. The vertical length of the well is 3000 m and the horizontal length of the well is 3000 m. The horizontal part is placed at 3000 m depth. The radius of curvature for the joint connecting the vertical and horizontal parts is 60 m. A 1–V voltage source is inserted into

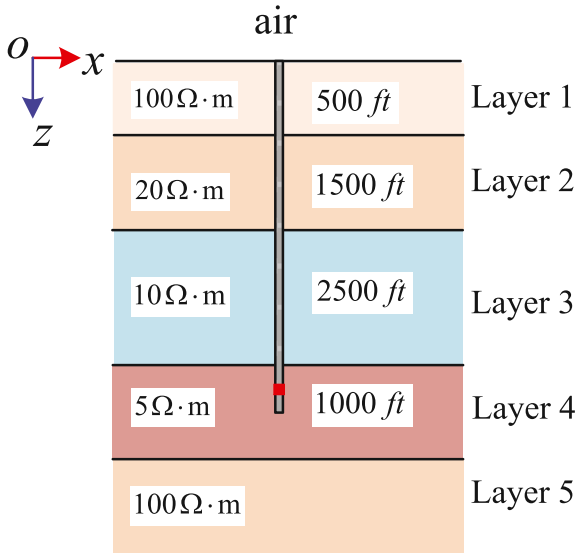

Fig. 3. A 5000 ft vertical drill string inserted into a five-layer formation.

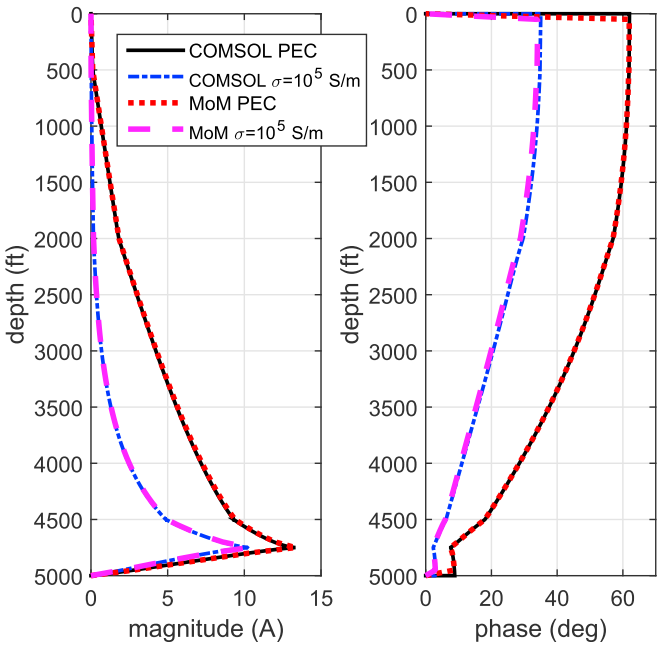

Fig. 4. Magnitude (left) and phase (right) of electric current distribution on a 5000 ft vertical drill string for two cases: drill string is perfect electric conductor (PEC) and drill string is of finite conductivity ($\sigma = 10^5$ S/m).

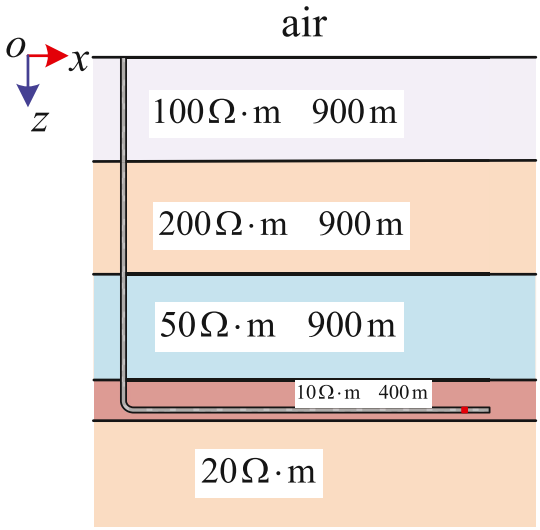

Fig. 5. A horizontal well drilling into a five-layer formation. The resistivity and thickness of each layer are labeled. The length of the vertical portion of the well is 3000 m. The length of the horizontal portion is 3000 m. A voltage source is placed near the drill bit.

the pipe at 100 m away from the drill bit and its direction is parallel to the pipe. The frequency of the source is 5 Hz. Similar to the case of vertical well, Fig. 6 shows the magnitude and phase of the current distribution on the pipe when the radius of pipe is 5 in. The results of our method and COMSOL fit well for the whole well. The little discrepancy for the phase of current distribution is the dispersion error caused by FEM. Table 1 compares the computational costs for COMSOL and MoM, from which we can see that the MoM is much more efficient than FEM in modeling EM telemetry for the realistic horizontal well. The proposed method shows fast and efficient modeling for very deep measurements.

In EM telemetry systems, the magnitude of the detected voltage signal at the surface largely depends on the operating frequency and the underground resistivity profile. Here we examine how the operating fre-

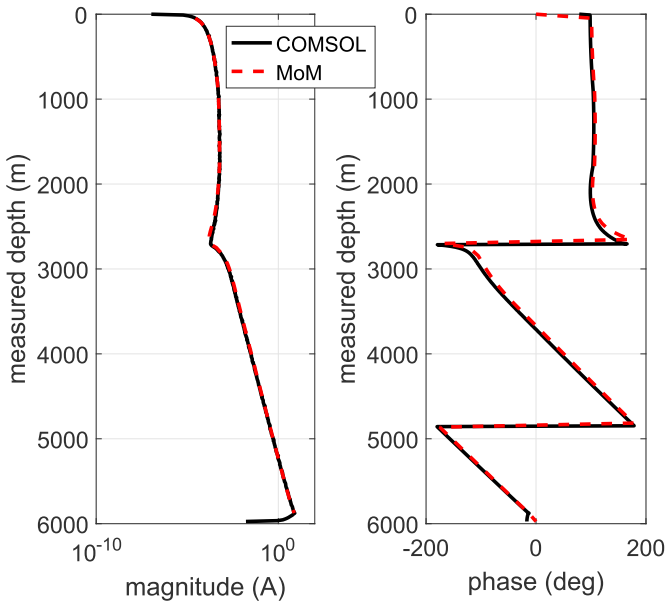

Fig. 6. Magnitude (left) and phase (right) of the electric current distribution on the drill string.

Table 1
Computational costs of COMSOL and MoM for the scaled horizontal drilling.

	number of unknowns	memory cost	CPU time
COMSOL	45479288	176 GB	151 min
MoM	139	2.5 MB	87 s

quency and resistivity profile affect the amplitude of the voltage received at the formation surface. Fig. 7 shows a directional drill string in a three-layer formation. The vertical portion of the drill string is 5000 ft long, while the horizontal portion is 3000 ft long. Thicknesses of Layers 1 and 2 (the target layer) are 4900 ft and 200 ft, respectively. The 1–V source is located on the drill string 200 ft away from the drill bit. The resistivities of Layers 1–3 are 20 Ω· m, 100 Ω· m, and 20 Ω· m, respectively. The operating frequency is 5 Hz and the radius of the drill string is 5 in. The surface receiver is deployed to detect the voltage drop between the wellhead and a point on the surface 300 ft away and in the same direction as the horizontal part of the drill string, as shown in Fig. 7.

Since FEM is so inefficient in modeling 3D telemetry, in field practices a horizontal or deviated well is often approximated to a vertical well with rotations to all the non-vertical segments. Then 2.5D FEM instead of 3D FEM can be used to model the simplified vertical well. Apparently this strategy will save a great amount of computational cost by FEM, but at the expense of losing accuracy. On the other hand, the proposed method in this paper can always model EM telemetry with high efficiency, no matter the well is vertical or deviated. The current distributions in both the simplified vertical drilling and the actual horizontal drilling are shown in Fig. 8, from which we can observe substantial differences between these two scenarios. Actually, the numerical result of received signal is 16.5 mV for the realistic horizontal drilling case, while it is 13.0 mV in simplified vertical drilling case. Using the proposed methodology, we thus obtain an accurate evaluation for the directional drilling case without resorting to the vertical well simplification.

In general, the depth of EM investigation in conductive formation can be approximated by the skin depth

$$\delta = \sqrt{\frac{2}{\omega\mu\sigma}}. \tag{20}$$

The signal measured at the surface decreases in amplitude with depth

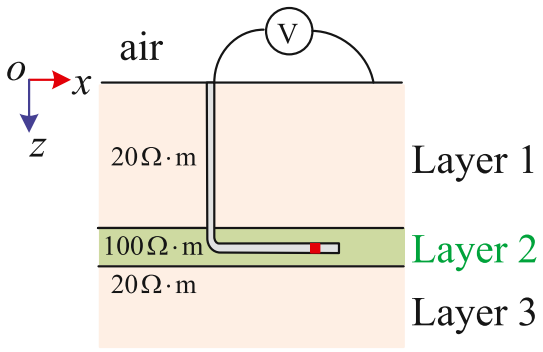

Fig. 7. Horizontal drilling in a three-layer formation.

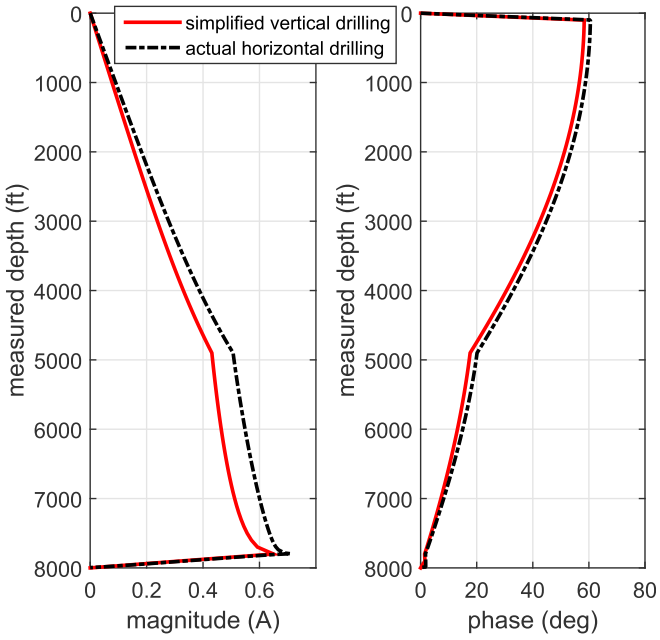

Fig. 8. Current distributions of simplified vertical drilling and of actual horizontal drilling.

by $e^{-d/\delta}$, where d is the depth. Decreasing the frequency results in increasing signal strength. However, it also reduces the bandwidth of the telemetry system. Therefore, the frequency of EM telemetry must be balanced against maximum well depth. The mud type is another problem to be considered for EM telemetry. In principle, compared to water-based mud, oil-based mud has beneficial effect on the signal strength (Schnitger et al., 2009).

Fig. 9 and Fig. 10 show current distributions and received signal strengths versus operating frequencies, respectively. The simulation results suggest that the received signal level has very minor changes when the frequency is below 1 Hz. As the frequency increases, however, the magnitude of the received signal begins to decrease, becoming undetectable at sufficiently high frequencies. If the noise level at the surface is 1 mV, the appropriate working frequency for EM telemetry in Fig. 7 will be below 20 Hz. When EM telemetry is used for very deep measurements, the working frequency should be much lower if only surface antenna or voltage meter is deployed to detect the transmitted signal. To enhance the amplitude of the received signal, several emerging techniques can be employed. One way is to use the steel casing of adjacent completed well as one electrode (Zeng et al., 2017). Since the steel casing of adjacent well is much nearer to the source, the magnitude of received signal can be enhanced by 10 times and more compared to conventional surface antenna. Another way is to employ the so-called deep electrode technique

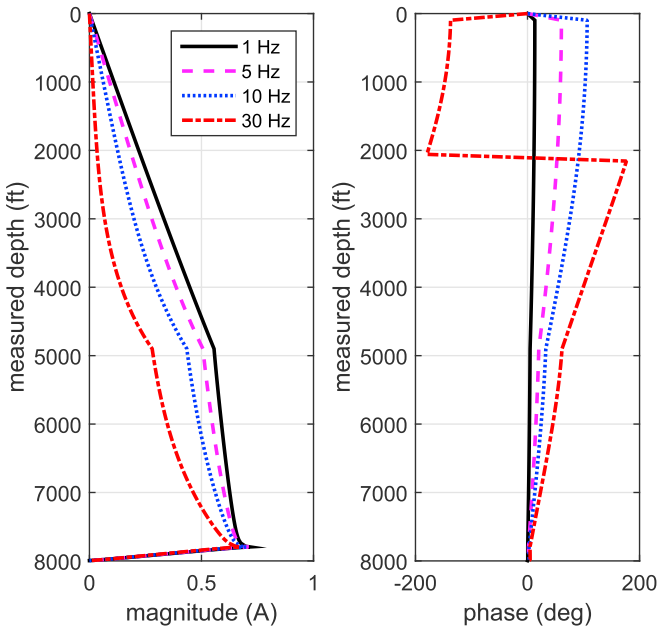

Fig. 9. Current distributions vs. operating frequency.

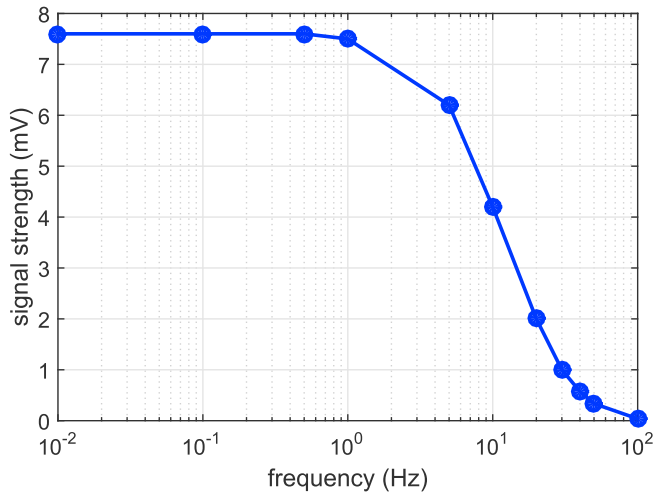

Fig. 10. Magnitude of received signal vs. operating frequency.

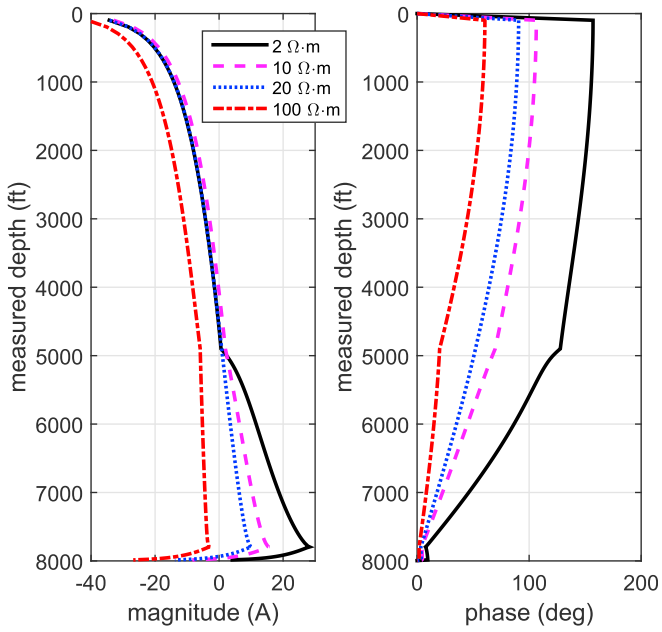

Fig. 11. Current distributions vs. target layer resistivity.

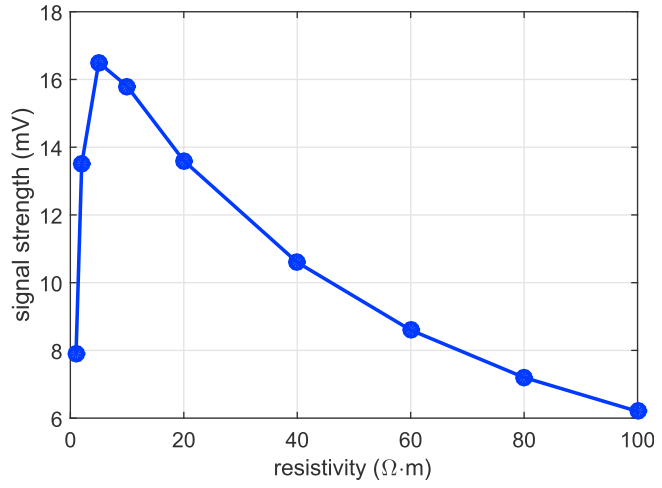

Fig. 12. Magnitude of received signal vs. target layer resistivity.

which deploys a wireline cable in an adjacent well and measures the potential difference between the bottom of the cable and the wellhead (Jannin et al., 2017). Relay of transceivers can also be applied to EM telemetry to obtain stronger signal (Li et al., 2016). These techniques can improve the working frequency of EM telemetry and is able to prosper the commercial applications of EM telemetry.

Fig. 11 and Fig. 12 show current distributions and received signal strengths versus resistivity of the layer containing the horizontal portion of the drill string (Layer 2 in Fig. 7), respectively. The operating frequency is fixed at 5 Hz. This example suggests that the conductivity of the target layer will affect the receivability of an EM telemetry system. Hence, when water flooding or hydraulic fracturing happens in the target layer, the magnitude of received signal by EM telemetry will be influenced. How the water flooding and hydraulic fracturing influence the EM telemetry should rely on other numerical methods and will be our future work.

To further validate our method for modeling EM telemetry, the last example is a field case of vertical drilling done in Oklahoma. The 1-A current source is working at 5.33 Hz and the radius of the drill string is 3.375 in. Fig. 13 shows the resistivity log of this job from the surface to 5000 ft and the magnitude of the simulated results for EM telemetry by our method compared to the actual measured signal for EM telemetry in field operations when the pipe is drilling down. As shown in Fig. 13, the calculated strength by our method has a very similar pattern to the measured signal within a large depth range. One should note that the discrepancies between the numerical results and actual measurements are unavoidable since environmental factor and borehole effects can affect the measured signal detected at the surface. Anyway, our method shows good efficiency and reasonable accuracy for this field case.

4. Conclusion

We have proposed a fast and accurate methodology to simulate EM telemetry systems in directional drilling. In principle, the method can be applied to a drill string with arbitrary trajectory inserted into a formation with numerous layers of horizontally stratified media. The method is used to analyze both vertical and horizontal wells, as well as the receivability of signals in a directional drilling scenario. Both numerical studies and field case are presented to verify the proposed approach. The

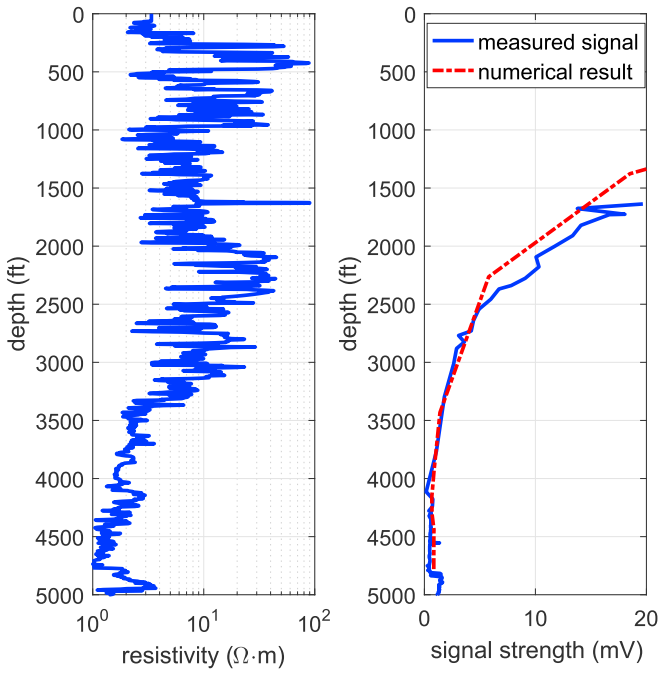

Fig. 13. Resistivity log (left) and received EM telemetry signal at the surface (right) for a vertical drilling done in Oklahoma.

conventional EM telemetry which only use a surface receiver is not sufficient for very deep measurement. Casing and crosswell technique can be used to increase the amplitude of the EM telemetry signal. Meanwhile, the operations of water flooding and hydraulic fracturing can affect the amplitude of the received signal.

Acknowledgement

The authors would like to thank Weatherford for the permission to publish their field case.

References

Bhagwan, J., Trofimenkoff, F.N., 1982. Electric drill stem telemetry. IEEE Trans. Geoscience Remote Sens. GE-20, 193–197. https://doi.org/10.1109/TGRS.1982.350397.

Champagne, N., 1996. A Three-dimensional Method of Moments Formulation for Material Bodies in a Planar Multi-layered Medium. Ph.d. dissertation. Univ. of Houston.

Chen, J., Zeng, S., Dong, Q., Huang, Y., 2017. Rapid simulation of electromagnetic telemetry using an axisymmetric semianalytical finite element method. J. Appl. Geophys. 137, 49–54. https://doi.org/10.1016/j.jappgeo.2016.12.006.

DeGauque, P., Grudzinski, R., et al., 1987. Propagation of electromagnetic waves along a drillstring of finite conductivity. SPE Drill. Eng. 2, 127–134. https://doi.org/10.2118/12943-PA.

Felsen, L.B., Marcuvitz, N., 1994. Radiation and Scattering of Waves. John Wiley & Sons.

Harrington, R.F., Harrington, J.L., 1996. Field Computation by Moment Methods, first ed. Oxford University Press.

Hill, D.A., Wait, J.R., 1978. Electromagnetic basis of drill-rod telemetry. Electron. Lett. 14, 532–533. https://doi.org/10.1049/el:19780361.

Itoh, T., 1980. Spectral domain immitance approach for dispersion characteristics of generalized printed transmission lines. IEEE Trans. Microw. Theory Tech. 28, 733–736. https://doi.org/10.1109/TMTT.1980.1130158.

Jannin, G., Chen, J., DePavia, L.E., Sun, L., Schwartz, M., 2017. Deep electrode: a game-changing technology for electromagnetic telemetry. In: SEG Technical Program Expanded Abstracts 2017. Society of Exploration Geophysicists, pp. 1059–1063. https://doi.org/10.1190/segam2017-17731164.1.

Li, W., Nie, Z., Sun, X., 2016. Wireless transmission of mwd and lwd signal based on guidance of metal pipes and relay of transceivers. IEEE Trans. Geoscience Remote Sens. 54, 4855–4866.

Li, W., Nie, Z., Sun, X., Chen, Y., 2014. Numerical modeling for excitation and coupling transmission of near field around the metal drilling pipe in lossy formation. IEEE Trans. Geoscience Remote Sens. 52, 3862–3871. https://doi.org/10.1109/TGRS.2013.2277231.

Michalski, K.A., 1998. Extrapolation methods for sommerfeld integral tails. IEEE Trans. Antennas Propag. 46, 1405–1418. https://doi.org/10.1109/8.725271.

Michalski, K.A., Mosig, J.R., 1997. Multilayered media green's functions in integral equation formulations. IEEE Trans. Antennas Propag. 45, 508–519. https://doi.org/10.1109/8.558666.

Michalski, K.A., Zheng, D., 1990. Electromagnetic scattering and radiation by surfaces of arbitrary shape in layered media. i. theory. IEEE Trans. Antennas Propag. 38, 335–344. https://doi.org/10.1109/8.52240.

Schnitger, J., Macpherson, J.D., et al., 2009. Signal attenuation for electromagnetic telemetry systems. In: SPE/IADC Drilling Conference and Exhibition. Society of Petroleum Engineers.

Sommerfeld, A., 1949. Partial Differential Equations in Physics. Elsevier Science.

Wei, Y., Holter, B., Simonsen, I., Husby, K., Kuhnle, J., Norum, L., 2010. Wave propagation along a thin wire antenna placed in a horizontally layered medium. In: Electromagnetic Field Computation (CEFC), 2010 14th Biennial IEEE Conference on. IEEE, 1–1.

Wilton, D.R., Champagne, N.J., 2006. Evaluation and integration of the thin wire kernel. IEEE Trans. Antennas Propag. 54, 1200–1206. https://doi.org/10.1109/TAP.2005.872569.

Xia, M.Y., Chen, Z.Y., 1993. Attenuation predictions at extremely low frequencies for measurement-while-drilling electromagnetic telemetry system. IEEE Trans. Geoscience Remote Sens. 31, 1222–1228. https://doi.org/10.1109/36.317441.

Yang, W., Torres-Verdn, C., Hou, J., Zhang, Z.I., 2009. 1d subsurface electromagnetic fields excited by energized steel casing. Geophysics 74, E159–E180. https://doi.org/10.1190/1.3131382.

Yla-Oijala, P., Taskinen, M., 2003. Efficient formulation of closed-form green's functions for general electric and magnetic sources in multilayered media. IEEE Trans. Antennas Propag. 51, 2106–2115. https://doi.org/10.1109/TAP.2003.814738.

Zeng, S., Dong, Q., Chen, J., 2017. A novel casing antenna system for crosswell electromagnetic telemetry in pad drilling. In: Unconventional Resources Technology Conference (URTEC), pp. 430–435.